IPNO-DR 99-25

Study of spallation residues by the reverse kinematics method in the reaction Au + p at 800 AMeV

B. Mustapha, F. Farget, L. Tassan-got, C. Stéphan, M. Bernas
P. Armbruster, T. Enqvist, K.-H. Schmidt, J. Taieb
J. Benlliure
A. Boudard, R. Legrain, S. Leray, C. Volant, W. Wlazlo
S. Czajkowski, J.P. Dufour, M. Pravikoff

Contribution to the XXXVII Bormio conference
Italy, January 1999

Study of spallation residues by the reverse kinematics method in the reaction Au + p at 800 AMeV

B. Mustapha, F. Farget, L. Tassan-got, C. Stéphan, M. Bernas
IPN Orsay, IN2P3,F-91406 Orsay, France
P. Armbruster, T. Enqvist, K.-H. Schmidt, J. Taieb
GSI, Planckstraße 1,D-64291 Darmstadt, Germany
J. Benlliure
University of Santiago de Compostela, E-15706 Santiago de Compostela, Spain
A. Boudard, R. Legrain, S. Leray, C. Volant, W. Wlazlo
DAPNIA/SPhN CEA/Saclay F-91191 Gif-sur-Yvette CEDEX, France
S. Czajkowski, J.P. Dufour, M. Pravikoff
CENBG, IN2P3,F-33175 Gradignan, France

Abstract

Production cross sections and momentum distributions of spallation residual nuclei were measured in the reaction Au + p at 800 AMeV in reverse kinematics. The experiment was performed at GSI-Darmstadt using the fragment separator FRS. The results are compared to earlier data and to model calculations. They are analysed in the frame of the two-step model : intranuclear cascade + evaporation. The excitation energy, deposited in the first step, is discussed.

I- Introduction

The nuclear interaction of a light particle (n, p, d, ...) with a heavy nucleus at relativistic energies leads to the emission of many neutrons and other light particles leaving a residual nucleus. It was proven that such reactions called "spallation" are responsible for changes in the nuclear composition of cosmic rays [1]. The same phenomenon would take place in the spallation target of a future accelerator-driven reactor, aimed at incinerating nuclear waste [2,3], where the spallation reaction would be used as a neutron source. The spallation residues could contribute to the radiotoxicity and to the neutron absorption. Furthermore, they could affect the thermal behaviour

of the reactor and induce the chemical corrosion of its vessel. It is thus necessary to assess their production yields. Their recoil-velocity distribution are also of interest to evaluate damages in materials.

The existing data obtained by γ-spectrometry methods [4] on targets irradiated by proton beams are, generally, limited to cumulative yields of long-lived and medium-lived species, due to radioactive decay. More complete and accurate data are necessary for application purposes and to improve our understanding of the spallation mechanism in order to elaborate more realistic model calculations.

The availability of relativistic heavy-ion beams at GSI makes possible the study of spallation residues using the reverse kinematics. The spectrometer FRS [5] allows their in-flight identification in mass and in nuclear charge before any radioactive decay. Their velocities are determined by a time-of-flight measurement.

The two next sections (II, III) deal with the experimental conditions and the data analysis. In section (IV), results about production cross sections will be presented and compared to earlier data. A discussion in the frame of the two-step model will also be given by comparing experimental results with two different Intranuclear cascade + Evaporation calculations. The recoil properties of spallation residues will be discussed in section (V). Our conclusions will be given in section (VI).

II- Experiment

A ^{197}Au beam accelerated by the heavy-ion synchrotron SIS to 800 AMeV, was impinging on a liquid-hydrogen target [6] installed in the reaction chamber at the entrance of the fragment separator FRS [5]. The hydrogen target thickness was measured at working conditions to be 12.4 $\pm$ 0.3 mm (87.5 $\pm$ 2.2 mg/cm^2). Four titanium foils of 20 μm enclosed the target, corresponding to a total thickness of 36 mg/cm^2. A niobium foil of 60 mg/cm^2 was used as a stripper behind the target in order to increase the probability of fully stripped ions.

The FRS is a forward two-stage magnetic spectrometer, characterized by a dispersive intermediate focal plane (S_2) and different operation modes. In this experiment, the FRS was operating in its achromatic mode, allowing the isotopic separation of the reaction products. Up-stream to the target position, a Secondary Electron Emission TRAnsmission Monitor SEETRAM [7] measured the beam intensity. At S_2, a thick wedge-shaped energy degrader (3.5 g/cm^2 eq. Al) was used in order to increase the resolution in the charge-state discrimination [8]. The slowing-down effect in the degrader combined with the magnetic deviation in the second stage of the FRS restricts the transmission to a narrow range of nuclear charges Z. Therefore, it is possible to tune the beam intensity according to their production cross sections and insure that all isotopes are measured with approximately the same statistical error. Moreover, the energy loss in the degrader could be calculated and used as an independent measurement of the nuclear charge Z.

Two position-sensitive plastic scintillators [9] located at the intermediate and at the final focal planes, respectively, provide the time-of-flight (ToF) and position measurements. The final focal plane (S_4) was also equipped with a multisampling ionisation chamber, MUSIC [10], measuring the energy loss in order to determine the charge Z. Two multiwire chambers were also used for tracking purposes and angle determina-

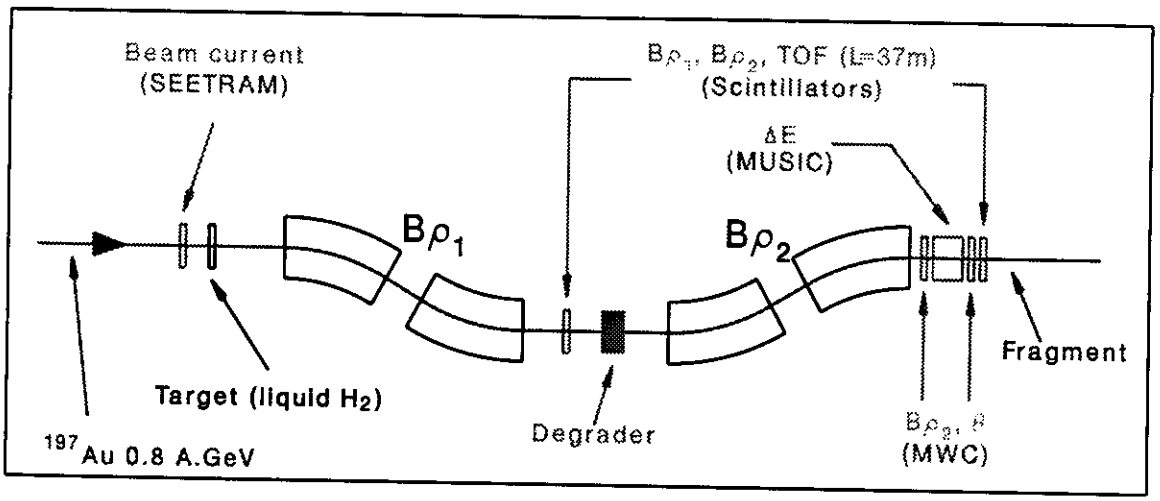

Figure 1: *Setup of the FRS.*

tion.

In this study, we deal with spallation residues, namely, residues with a mass loss, ΔA with respect to the projectile, less than 70. These residues have still a velocity close to the projectile velocity. Assuming an isotropic momentum distribution in the projectile rest frame, the corresponding angular spread can be estimated from the width of the longitudinal momentum distribution, $\sigma_{p_{//}}$. For a mass loss of $\Delta A = 50$, the angular dispersion is estimated to be $\sigma_\theta \sim 3\ mrad$ ($\sigma_\theta = \mathrm{Atan}(\frac{\sigma_{p_{//}}}{p_{beam}})$), which is well within the angular acceptance of the FRS ($\pm$ 15 $mrad$). Therefore, the entire angular distribution of spallation residues is covered. Since the momentum acceptance of the FRS is about 2 %, several magnetic field settings were necessary to span all produced residues. To subtract the contribution of titanium and niobium foils to the total fragment production, some other settings were done with an equivalent target.

III- Data analysis

From the positions measured at S_2 and S_4, the magnetic rigidities in the first ($(B\rho)_1$) and the second ($(B\rho)_2$) stage of the FRS, could be deduced for each detected fragment. Combining this information to the time-of-flight ToF in the second half of the spectrometer and the energy loss ΔE in MUSIC, the identification of all isotopes could be achieved. However, for high nuclear charges, the fraction of not fully stripped ions is still significant (q=Z $\sim$ 90%, q=Z-1 $\sim$ 10%, lower charges are negligible) and may introduce ambiguities in the identification.

III-1 Identification of fragments

The energy loss in MUSIC of a high-energy heavy ion depends, in addition to its

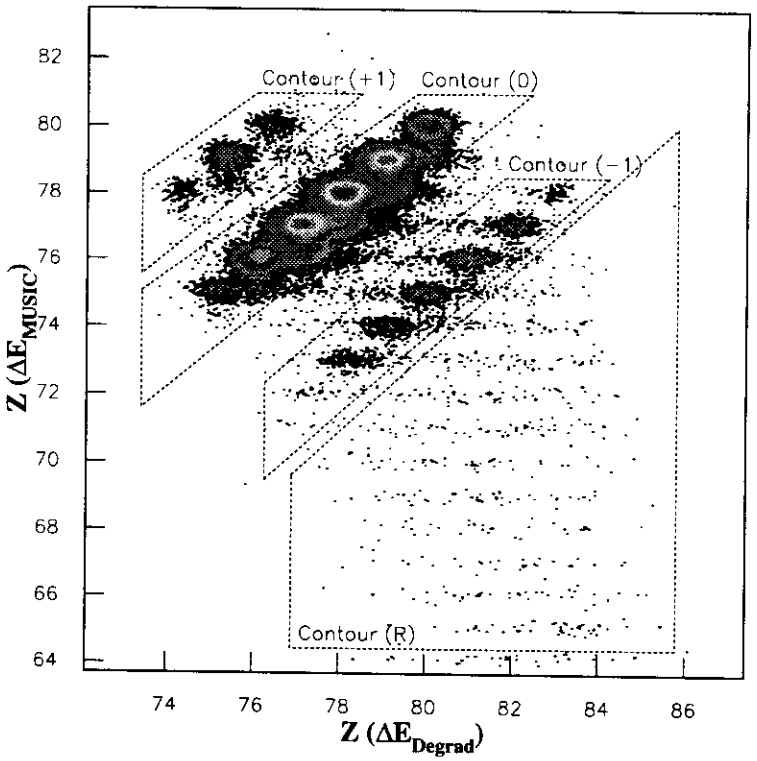

Figure 2: *Z identification : The Z axis refer to the main diagonal (contour 0) only.*

nuclear charge, Z, on changings of its atomic charge state across the MUSIC gas, spoiling in this way the Z determination. The energy loss in the degrader deduced from the change in magnetic rigidity $(B\rho)_1$ - $(B\rho)_2$, provides an independent measurement of the nuclear charge, since its thickness is sufficient to obtain a charge-state equilibrium. The Z determination is then achieved by the correlation of both energy losses in MUSIC and in the degrader, see figure 2.

In figure 2, the main diagonal (contour 0) corresponds to fully stripped ions ($q_1 = q_2 = Z$, q_1 and q_2 are charge states before and after the degrader) without changing the charge state across the degrader. The upper (contour +1) and the lower (contour -1) diagonals refer, respectively, to ions gaining ($q_1 = Z$, $q_2 = Z\text{-}1$) or loosing ($q_1 = Z\text{-}1$, $q_2 = Z$) one electron in the degrader. The scattered events below the diagonals (contour R) are associated to secondary nuclear reaction fragments produced in the degrader. These events are rejected. Only events from contour (0) are used to evaluate cross sections and events from contour (1) and (-1) are used to correct for charge-state changing.

From the time-of-flight in the second part of the FRS, we deduce the velocity of each residue. Using the charge identification (q_2), the mass is determined from the relation :

$$A = q_2 \times \frac{(B\rho)_2}{(\beta\gamma)_2} \; ; \; (unit\ system\ c = 1)$$

with β_2 being the velocity in the second half of the FRS and $\gamma_2 = 1/\sqrt{1-\beta_2^2}$, the corresponding Lorentz factor. Figure 3 shows the mass spectrum for Z = 77 for a specific magnetic- field setting.

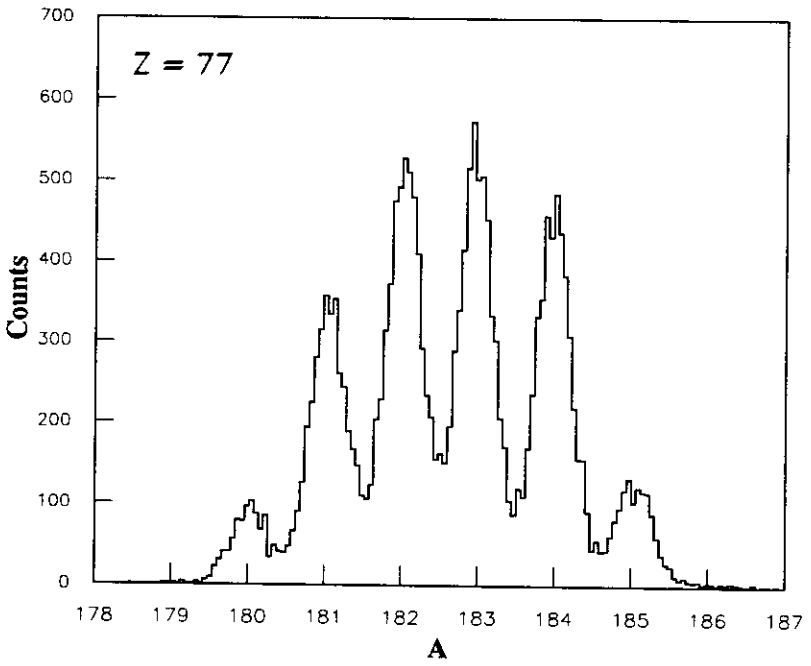

Figure 3: *Mass spectrum for Z=77 for a specific magnetic-field setting.*

III-2 Reconstruction of the momentum spectra

For an identified isotope (Z,A), it is possible to calculate event by event the momentum per mass unit, $(\beta\gamma)_1$, at the exit of the target, using the relation $(\beta\gamma)_1 = (B\rho)_1 \times Z/A$ and obtain in this way its momentum distribution. For residues far from the projectile, the momentum distribution becomes wider and could not be completely transmitted in one setting of the FRS. In this case, the full distributions could be obtained by superimposing contributions from settings with magnetic rigidity close to that of the considered nuclei. Counting rates should, firstly (before superimposition), be corrected for the respective dead time and normalized to the corresponding number of incident ^{197}Au nuclei on the target. By this way we can also check the consistency between different settings.

Figure 4 shows the two extreme cases : (a) A residue produced by the loss of ten nucleons ($\Delta A = 10$ with respect to the projectile), for which the momentum distribution is obtained from one setting. (b) A residue with $\Delta A = 50$ showing the broadening of the momentum distribution obtained by superimposing two different settings.

For cases where the momentum spectrum is still truncated, it was completed by a gaussian fit if most of the distribution is transmitted, if not, the relative events were rejected and no cross section was evaluated for the corresponding nuclei.

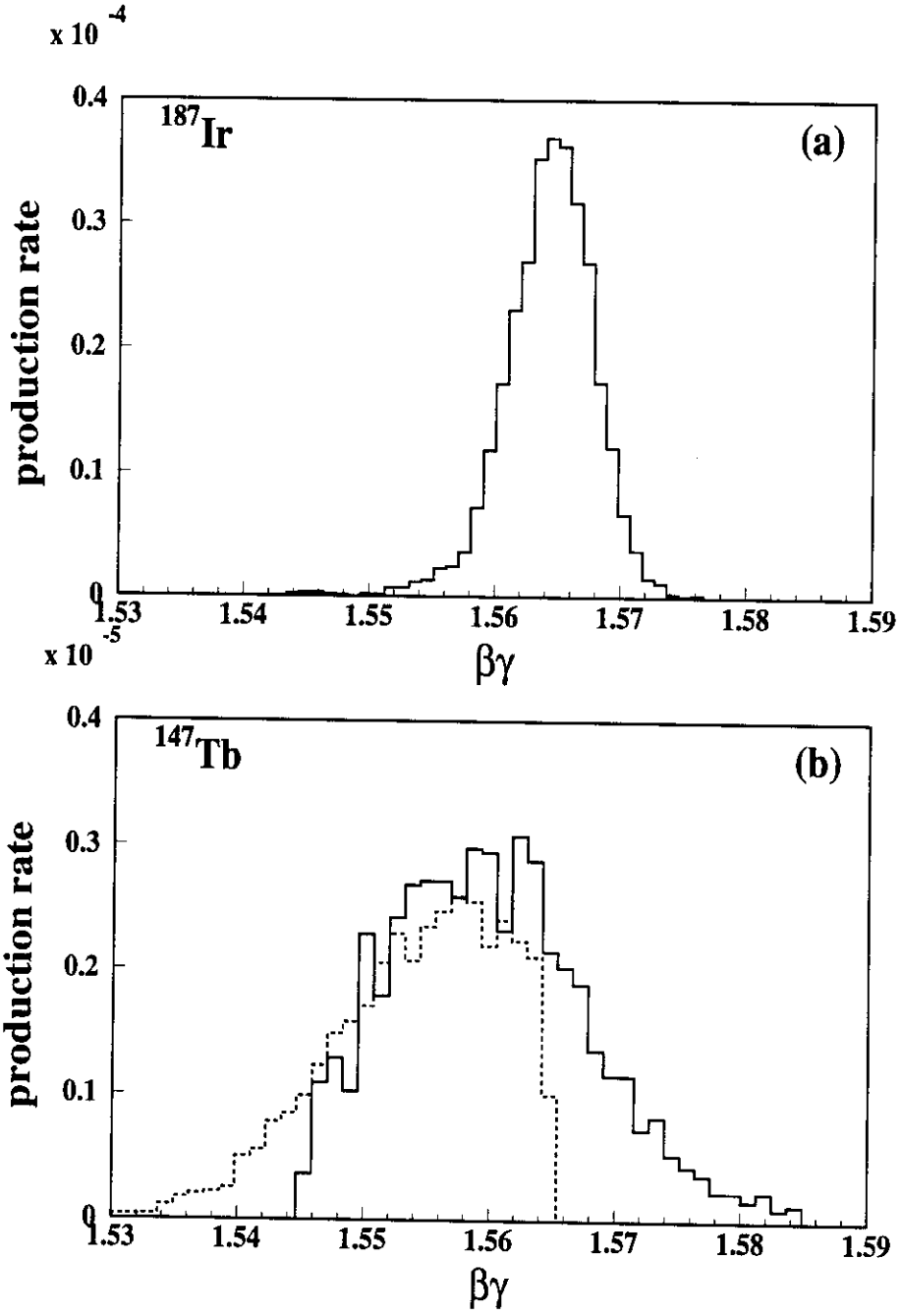

Figure 4: *Momentum spectrum reconstruction : (a) ΔA=10 and one setting was used to obtain the momentum spectrum, (b) ΔA=50 showing the consistency between the two settings (shown by the full and the dashed histograms) used to obtain the complete momentum distribution.*

III-3 Evaluation of cross sections

For a given residue (A,Z), the integration of the momentum distribution gives the production rate corrected only for dead-time :

$$r(A,Z) = \frac{N_{surviving}(A, Z, q_1 = q_2 = Z)}{N_{incident}(^{197}Au)}$$

where $N_{surviving}$ is the number of fragments surviving to charge-state changings and secondary reactions in the different layers of matter placed in the beam line. Hence, to obtain the corresponding cross section, several corrections had to be applied. Charge state changings and secondary reactions in the degrader, in the windows of the target and in the target itself had to be taken into account.

The fraction of fully stripped Au ions after the target is measured to be 92 % and to decrease to 80 % behind the degrader. For other ions, these fractions were calculated using a code [11] and scaled to the measured Au values.

The rate of secondary nuclear reactions of the primary beam ^{197}Au in the degrader was measured to be 33 %. For residues, this rate was estimated using a total cross section formula [12] renormalized to the primary beam value.

As mentioned before, some settings were done to measure the contribution of the target windows to the residue production. This contribution is very small ($\sim$ 3%) for residues close to the projectile, except for ^{196}Au residual nucleus for which it reaches 22% due to the electromagnetic dissociation. It becomes more important for lower masses (ΔA = 60) where it reaches 25%.

The secondary reactions in hydrogen itself are an important source of contamination, especially for low-mass residues which have more chance to be produced in two successive reactions. This contribution has been estimated from the obtained cross sections, assuming that the probability of loosing ΔA nucleons depends only on ΔA. Figure 5 shows the corrective factor to be applied to the measured cross section as a function of the loss of mass ΔA.

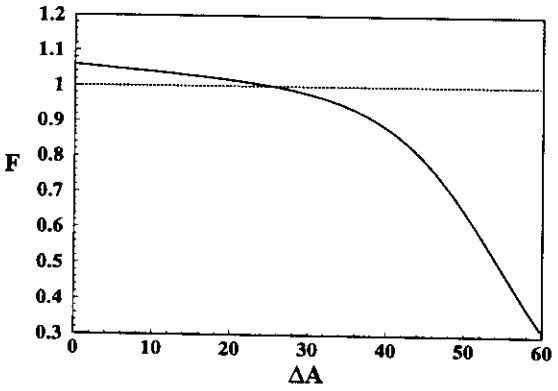

Figure 5: *Correction factor for secondary reactions in the target.*

Close to the projectile this factor is greater than 1 because secondary reactions deplete this region. However, it drops steeply at large mass loss (ΔA > 50), indicating that most of the production of the corresponding residues originates from secondary reactions.

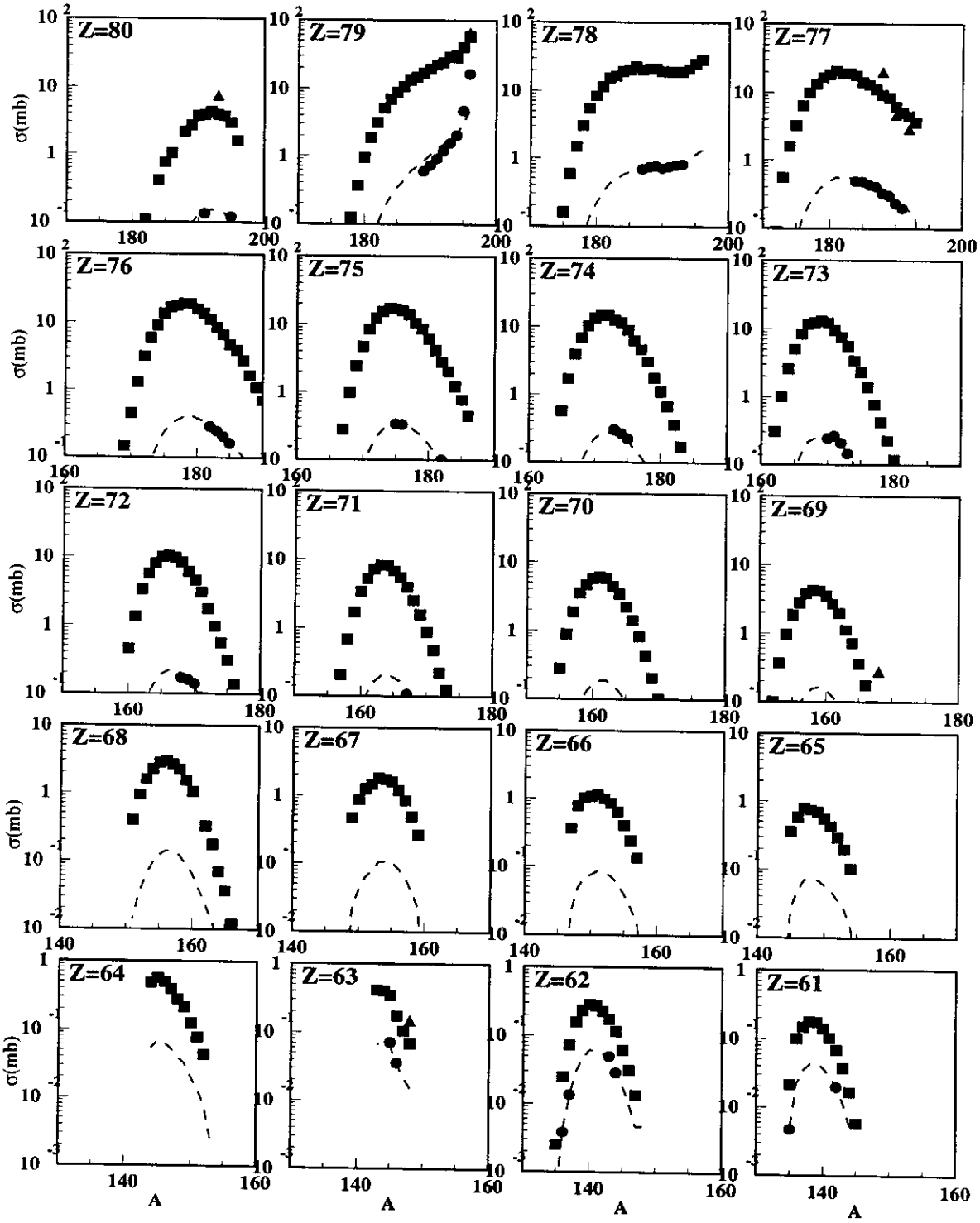

Figure 6: *Isotopic cross sections of residues from spallation of gold in hydrogen at 800 AMeV (squares), the circles and the dashed curves (interpolation) refer to the corresponding fraction produced in the target windows. The few independent cross sections from radiochemical data are shown by triangles.*

IV- Production cross sections

Results concerning cross sections are reported on figure 6. The smoothness of the isotopic distributions (squares) indicates that cross sections are determined with a high relative accuracy; from one isotope to the other the error does not exceed 5 %. But a systematic error of 10 to 15 % is estimated for the whole set of residues. This error could be larger, about 40 %, for lower mass residues (A $<$ 150) due to the contamination by secondary reactions in the target.

The full circles show the fraction produced in the windows of the target measured only for few isotopes. For residues not covered by these measurements an interpolation was performed (dashed lines).

The scarce independent cross sections taken from the work of Michel et al [4] obtained by radiochemical methods are shown by triangles. A wider comparison between our data and radiochemical data is given in the next subsection.

IV-1 Comparison to the existing data

Recent measurements by Michel et al [4] have been done by irradiating different targets with energetic proton beams at different energies. γ-Spectrometry and Accelerator Mass Spectrometry, were used to identify spallation residues. Such methods allow to detect only radioactive species at the end or in the course of the decay chains. Therefore, independent yields were obtained only for shielded isotopes : the direct products of the nuclear collision (triangles in figure 6). For isotopes produced partially by radioactive decay of their precursors, only cumulative yields were measured. Conversely in our case (reverse kinematics) all isotopes are detected and identified before any radioactive decay. Thus a direct comparison can only be performed for independent yields.

Figure 7 shows the ratio of our cross sections to the radiochemical ones for independent yields. The agreement is satisfactory except for the isotope ^{168}Tm for which the deviation factor of about ten is still unexplained. We should remind that in our case the relative yields are determined with a high accuracy (less than 5 %), therefore, regarding the fluctuations around R = 1 (fig 7), our data are probably more reliable and accurate.

To obtain from our data quantities equivalent to radiochemical cumulative yields, we have summed up cross sections over all nuclei leading by radioactive decay to the considered isotope. As the corridor of residues is shifted from the valley of β-stability to the neutron-deficient side, only β^+ and electronic capture decay had to be considered. The comparison of the obtained yields to the radiochemical ones (figure 8) shows an overall good agreement.

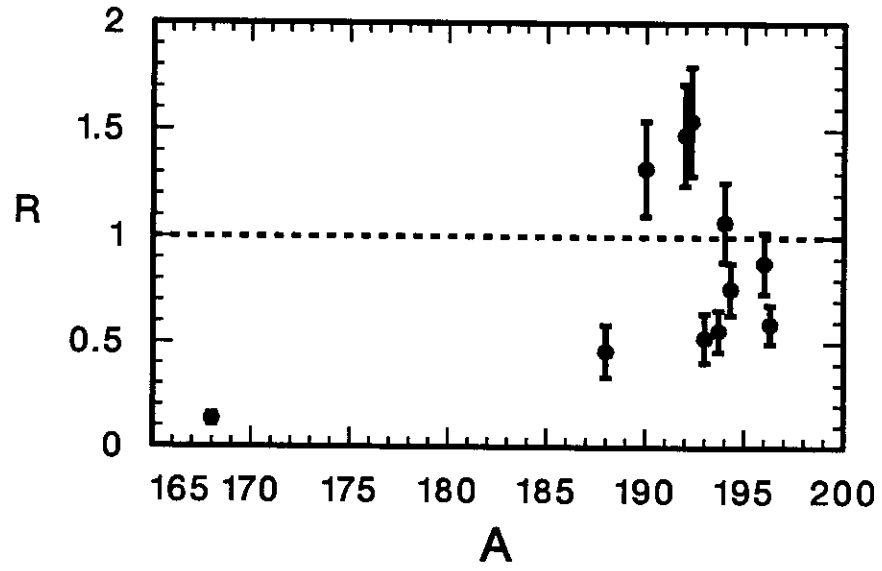

Figure 7: *Comparison with radiochemical data for independent yields : R is the ratio of our cross sections to radiochemical ones.*

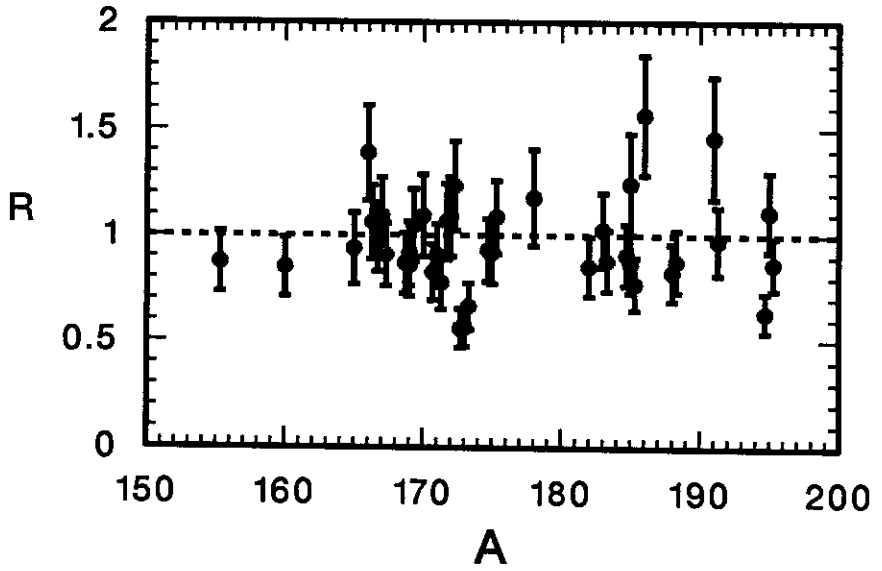

Figure 8: *Comparison with radiochemical data : same as fig. 7 but for cumulative yields.*

IV-2 Comparison to calculation models

A simple approach to calculate cross sections is to use a semiempirical parametrisation. We have performed calculations using the formula EPAX [13]. The result is compared to the experimental values in figure 9 for isobaric yields (σ(A)) and in figure 10 for isotopic distributions of some elements.

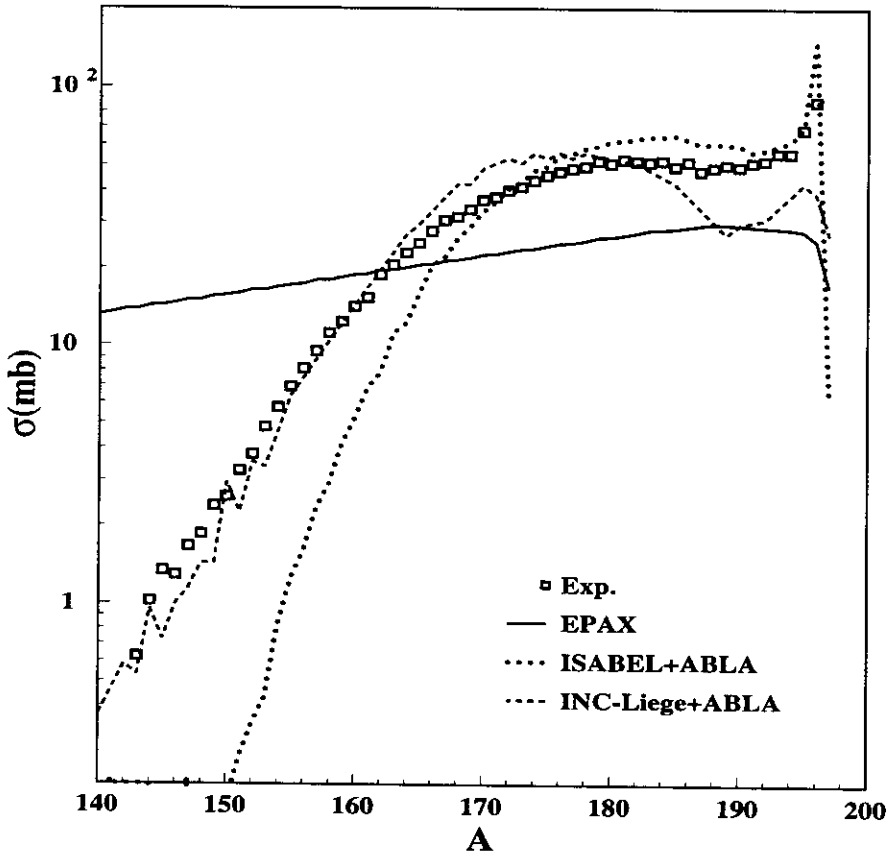

Figure 9: *Comparison with model calculations : Isobaric production cross sections.*

The disagreement seen for isobaric yields is due to the fact that the main condition on which this formula is based, the "limiting fragmentation", is not satisfied. The limiting fragmentation assumes that above an energy threshold, production cross sections do not depend on energy any more. If in the case of nucleus-nucleus collision, this condition is met at medium energies 200-300 MeV/n, for proton-nucleus collision it becomes true at much higher energies 2-3 GeV/n. From figure 10, one notes that the isotopic distributions from EPAX are shifted, with respect to experimental ones, towards the neutron-rich side (as in previous work [14]). This may reflect the lack of data which were available for the determination of the parameters. A new evaluation of the latter based on new data is given by K. Sűmmerer (this conference).

A more physical approach of the spallation process can be given in the frame of Serber's two step model [15]. A first fast step where some energetic particles are ejected leaves an excited prefragment. This step is well described by an intranuclear

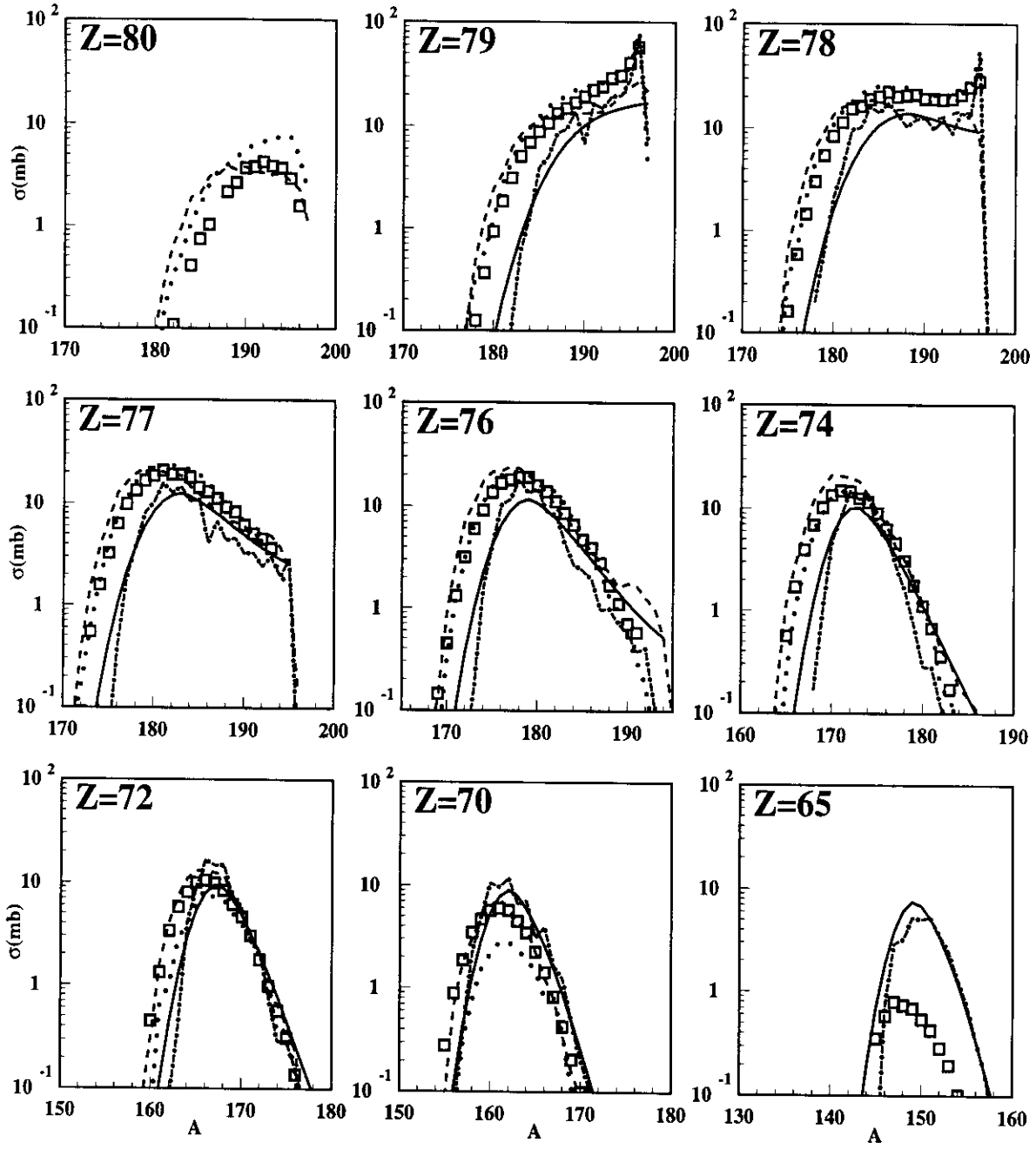

Figure 10: *Comparison with model calculations : Isotopic distributions.*

cascade of nucleon-nucleon interactions. The second step, which is a slower one, corresponds to the deexcitation of the prefragment by evaporating slow particles, mainly neutrons. The deexcitation by fission is also possible (J. Benlliure, this conference).

In order to examine the influence of the first step, we combined two different intranuclear-cascade calculations : ISABEL [16] and INC-Liège [17] with the same evaporation code : ABLA [18]. The comparisons to our experimental results are given in figures 9,10. It is shown in figure 9 that ISABEL underestimates the production of lower mass residues. INC-Liège seems to reproduce better the experimental results, however, its curve shows some distortions (the hollow around the mass 190 and the bump about 170) not seen in ISABEL. Due to the basic differences in the ISABEL and INC-Liège approaches, essentially in following cascade particles and in the criterion of stopping the cascade, important discrepancies appear in the excitation energy spectra of prefragments. INC-Liège's prefragments are, on average, more excited than ISABEL's ones. Knowing that higher excited nuclei evaporate more particles and give rise to lighter final fragments, we understand why ISABEL underestimates the production of lower masses. The higher excitation energy of INC-Liège prefragments close to the projectile (A $\sim$ 190) induces the depletion of this region and causes the overproduction of the corresponding fragments after evaporation, which have typically the mass A $\sim$ 170. Both calculations reproduce rather well the mean values and the widths of the isotopic distributions (figure 10).

In figure 10, is also shown the result of the LAHET calculation [19], which is a commonly used code based also on the two-step model. We note that this code behaves very similarly as EPAX and does not give a satisfactory agreement with the data.

V- Recoil properties of spallation residues

The recoil properties of the detected residue provide informations on the mechanism of its production. Using the method described in III-2, we obtained the recoil-momentum distribution for each residue. Figure 11 shows $\beta\gamma$-spectra of all osmium isotopes. Each of these distributions can be considered as Gaussian of mean value (the full line vertical arrow) shifted from the value corresponding to the primary beam (the dashed line vertical arrow). This shift corresponds to the recoil of the residual nucleus in the projectile rest frame, it reflects the violence of the collision leading to this residue. This explains the recoil increase with the loss of mass, lighter nuclei being produced in more violent collisions than those leading to residues close to the projectile. The recoil velocity gives then a measurement of the energy deposited during the collision and consequently of the prefragment excitation energy after the first step of the interaction. The evaporation step is supposed to contribute to the dispersion of the velocity distribution.

The mean recoil momentum for a given residue, in the projectile rest frame, is calculated using the definition given in [20] :

$$P'_{//} = m_{proj} < \beta_{//} > \beta_0\gamma_0/(\gamma_0 + 1)$$

where m_{proj} is the mass of the projectile and β_0 its velocity ($\gamma_0 = 1/\sqrt{1-(\beta_0)^2}$), $<\beta_{//}>$ is the mean longitudinal velocity of the residual nucleus in the projectile rest frame.

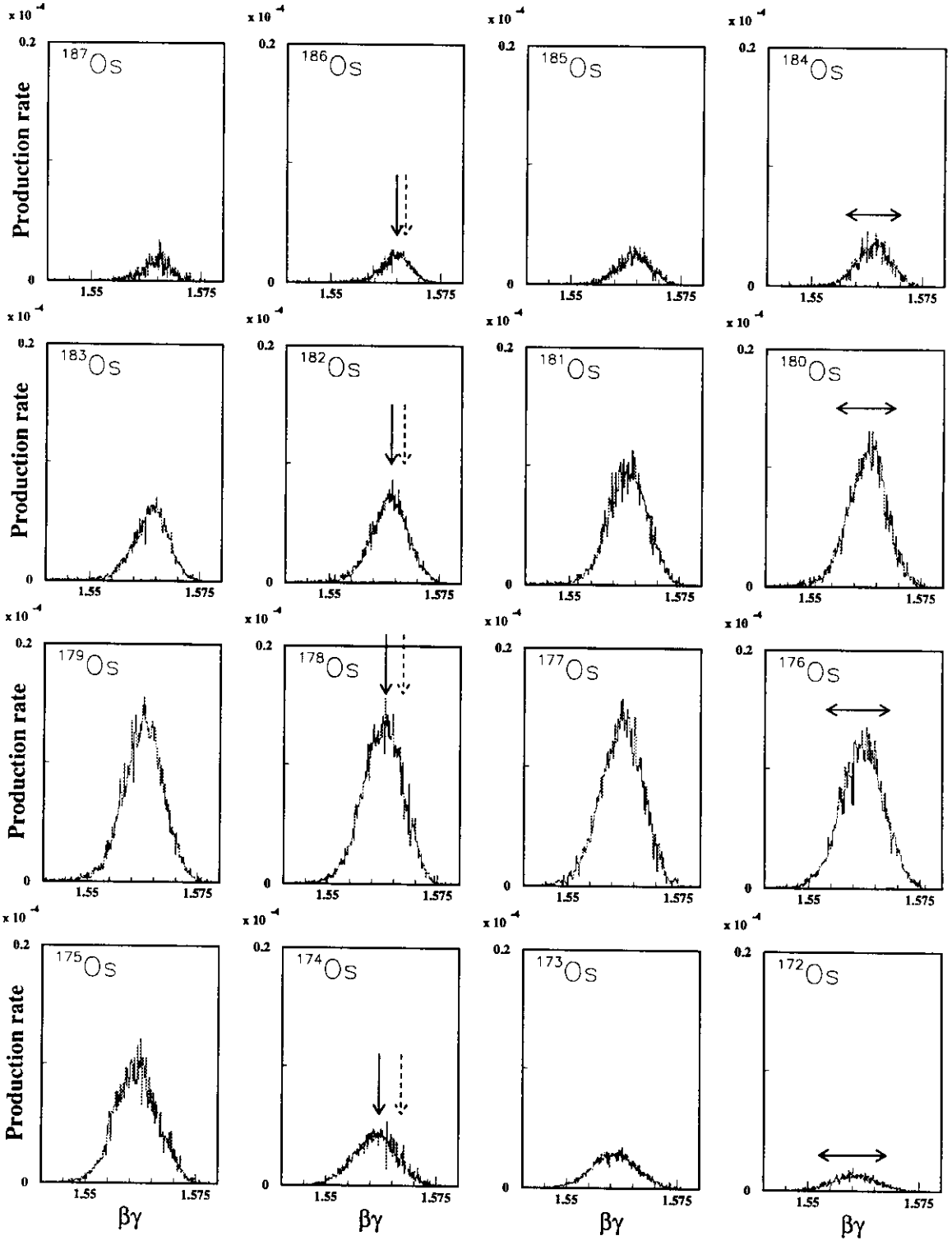

Figure 11: *$\beta\gamma$-spectra for Os-isotopes.*

The dispersion parameter of the momentum distribution is given by

$$P_{rms} = \sqrt{3} \times \sigma_{P_{//}}$$

where $\sigma_{P_{//}}$ is the standard deviation of the longitudinal momentum distribution and the factor $\sqrt{3}$ is to obtain the total dispersion (along the 3 directions).

Figure 12 shows the mean recoil momenta with respect to the projectile as a function of the loss of mass. The change in the slope seen around $\Delta A = 55$ could be due to secondary-reaction products in the target, for which the kinematics is completely different. In figure 13, the standard deviations show a linear dependence on the square root of the mass loss indicating somehow a statistical behavior in the emission of particles.

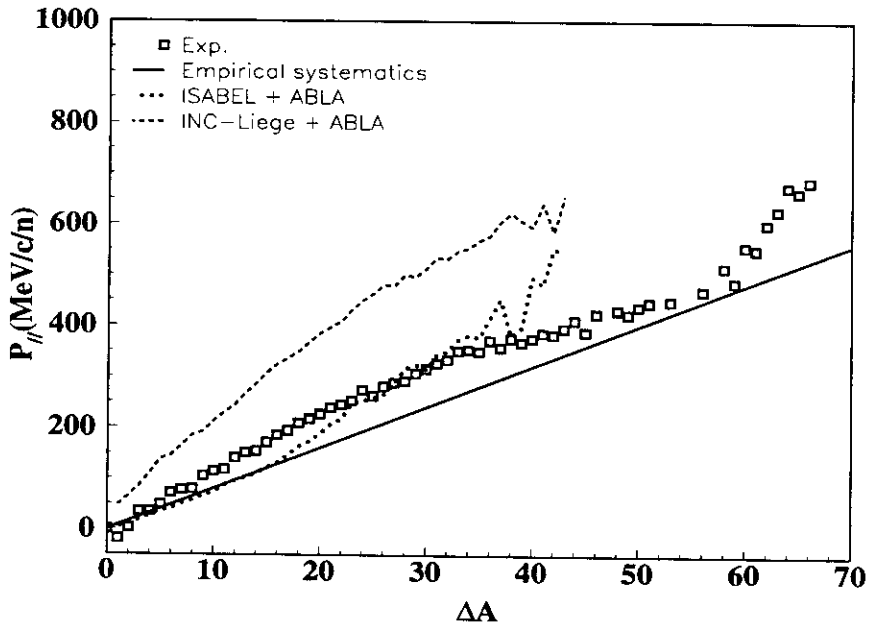

Figure 12: *The Mean recoil momentum, a comparison with empirical systematics and with model calculations.*

Compared to the empirical momentum systematics [20] based on nucleus-nucleus collision data, the recoil momentum seems to be slightly higher in the case of proton-nucleus collision (our case). This may due to the fact that the overlapping region of the collision partners is more important in the nucleus-nucleus system, this leads to more particle emission in the first step than in the proton-nucleus system. So, to reach the same mass loss, after the evaporation step, more excitation energy is needed in the case of proton-nucleus. Concerning the total standard deviations, P_{rms} (figure 13), no significant discrepancy is observed.

It is important to note from the same plots (figure 12,13), that the microscopic calculation ISABEL reproduces well the kinematics properties of the reaction. In contrast, the code INC-Liège overestimates significantly the mean recoil momenta, which can be related to the higher excitation energy deposited in the first step as previously mentionned.

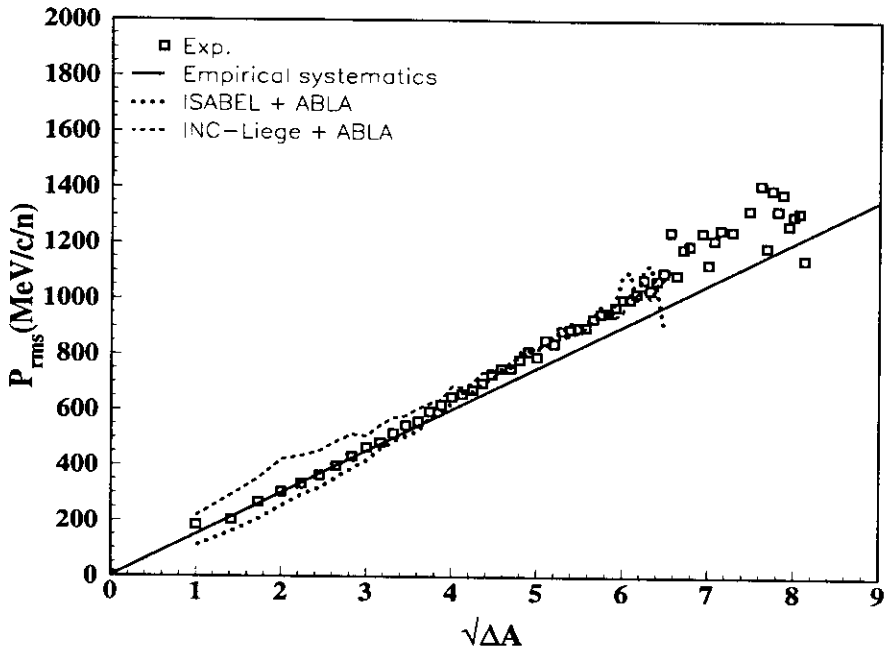

Figure 13: *The standard deviation of the recoil momentum distributions, a comparison with empirical systematics and with model calculations.*

VI- Conclusions

Production cross sections, before any radioactive decay, and momentum distributions of spallation residues from the reaction Au+p at 800 AMeV, were measured in reverse kinematics. Compared to earlier data obtained by radiochemical methods, our results show an overall agreement. However, our new data are more accurate and allow a more direct test for theoretical models. This kind of measurement has been extended to other spallation reactions : Pb+p (W. Wlazlo, this conference) and U+p (in progress). Unfortunately, up to now, neither model calculations nor semiempirical formulae, in their present forms, give a satisfactory agreement with the experimental data. In the calculation based on the two-step model : intranuclear cascade + evaporation, the energy deposition in the first step should be re-examined. The evaporation step has probably to be also refined. An empirical formula (as EPAX) including energy dependence could be very useful to reduce the calculation time. In order to simulate the production of residues in a thick spallation target, the real case of the hybrid system, further measurements at lower energies are scheduled by our group.

REFERENCES

[1] Silberberg R. and Tsao C.H., Phys. Rep. 191 N6 (1990) 351.
[2] Bowman C.D. et al, NIM A 320 (1992) 336.
[3] Rubbia C., report CERN AT 93-47 (ET).
[4] Michel R. et al, NIM B 129 (1997) 153.
[5] Geissel H. et al, NIM A 364 (1992) 150.
[6] Chesny P. et al, GSI annual report (1996) 190.

[7] Ziegler C. et al, GSI Scientific Report 1990, 91-1; Junghans A. et al, NIM A 370 (1996) 312.

[8] Dufour J. P. et al, NIM A 248 (1986) 267; Schmidt K. H et al, NIM A 260 (1987) 287.

[9] Voss B. et al, NIM A 364 (1995) 150.

[10] Pfűtzner M. et al, NIM B 86 (1994) 213.

[11] Scheidenberger C. et al, NIM B 142 (1998) 441.

[12] Kox S. et al, Phys. Lett. 159B N 1 (1985) 15.

[13] Sűmmerer et al, Phys. Rev. C 42 (1990) 2546.

[14] Benlliure J. et al, Eur. Phys. J. A 2 (1998) 193.

[15] Serber R., Phys. Rev. 72 N 11 (1947) 1114.

[16] Yariv Y. and Fraenkel Z., Phys. Rev. C 20 N 6 (1979) 2227.

[17] Cugnon J. et al, Nucl. Phys. A 620 (1997) 475.

[18] Gaimard J. J. and Schmidt K. H., Nucl. Phys. A 531 (1991) 709; Benlliure J. et al, Nucl. Phys. A 628 (1998) 458.

[19] Parel R. E. and Lichtenstein H., Los Alamos-UR-89-3014(1989).

[20] Morrissey D.J., Phys. Rev. C 39 N 2 (1989) 460.